SANDIA REPORT

SAND2013-8673
Unlimited Release
Printed September 2013

Environment Scattering in GADRAS

Gregory G. Thoreson, Dean J. Mitchell, Lisa A. Theisen, Lee T. Harding

Prepared by
Sandia National Laboratories
Albuquerque, New Mexico 87185 and Livermore, California 94550

Sandia National Laboratories is a multi-program laboratory managed and operated by Sandia Corporation, a wholly owned subsidiary of Lockheed Martin Corporation, for the U.S. Department of Energy's National Nuclear Security Administration under contract DE-AC04-94AL85000.

Sandia National Laboratories

Issued by Sandia National Laboratories, operated for the United States Department of Energy by Sandia Corporation.

NOTICE: This report was prepared as an account of work sponsored by an agency of the United States Government. Neither the United States Government, nor any agency thereof, nor any of their employees, nor any of their contractors, subcontractors, or their employees, make any warranty, express or implied, or assume any legal liability or responsibility for the accuracy, completeness, or usefulness of any information, apparatus, product, or process disclosed, or represent that its use would not infringe privately owned rights. Reference herein to any specific commercial product, process, or service by trade name, trademark, manufacturer, or otherwise, does not necessarily constitute or imply its endorsement, recommendation, or favoring by the United States Government, any agency thereof, or any of their contractors or subcontractors. The views and opinions expressed herein do not necessarily state or reflect those of the United States Government, any agency thereof, or any of their contractors.

SAND2013-8673
Unlimited Release
Printed September 2013

Environment Scattering in GADRAS

Gregory G. Thoreson, Dean J. Mitchell, Lisa A. Theisen, Lee T. Harding
Contraband Detection Department
Sandia National Laboratories
P.O. Box 5800
Albuquerque, New Mexico 87185-MS0782

Abstract

Radiation transport calculations were performed to compute the angular tallies for scattered gamma-rays as a function of distance, height, and environment. Green's Functions were then used to encapsulate the results a reusable transformation function. The calculations represent the transport of photons throughout scattering surfaces that surround sources and detectors, such as the ground and walls. Utilization of these calculations in GADRAS (Gamma Detector Response and Analysis Software) enables accurate computation of environmental scattering for a variety of environments and source configurations. This capability, which agrees well with numerous experimental benchmark measurements, is now deployed with GADRAS Version 18.2 as the basis for the computation of scattered radiation.

CONTENTS

1 Introduction 9
2 Methodology 11
2.1 Green's Functions 11
2.2 Application of Green's Functions to Surface Scattering 12
2.2.1 Single Surface Scattering 15
2.2.2 Multiple Surface Scattering 16
2.2.3 Computational Limitations 17
3 Implementation 19
3.1.1 Surface Scattering Simulation Data 19
3.2 Integration into GADRAS 19
3.2.1 Solid Angle Computation 21
3.2.2 Detector Shielding 21
3.2.3 Environment Definition 22
3.2.4 Interpolation Table 23
3.2.5 User Interface to Scatter Parameters 25
4 Testing and Benchmarking 27
5 Conclusions 33
6 References 35
Distribution 36

FIGURES

Figure 1. Direct and Indirect Radiation Paths 9
Figure 2. Photon Scattering Distance and Incident Energy 13
Figure 3. Scatter Angle Dimensions 14
Figure 4. Single Scattering Position on Surface 15
Figure 5. Integration of Scattering Surface 15
Figure 6. Double Integration of Two Scattering Surfaces 16
Figure 7. Detector Volume Arch 19

Figure 8. Scatter Surface Mesh 20
Figure 9. Two Surface Scatter Mesh 21
Figure 10. Environment File and Example Definition 23
Figure 11. Room Scattering as a Function of Distance and Height 24
Figure 12. Computed spectra (*red*) for the 3″×3″ NaI detector are compared with measurements (*black*) at a distance of 100 cm and height of 100 cm. 27
Figure 13. Computed spectra (*lines*) compared with measurements recorded by the HPGe detector at three distances (*dots*) at a height of 100 cm. 28
Figure 14. Computed spectra (*lines*) compared with measurements recorded by the HPGe detector at three heights (*dots*) at a distance of 100 cm. 29
Figure 15. Spectra recorded by the three detectors at the same distance (100 cm) and height (100 cm). 29
Figure 16. Comparison of Computed versus Measured Scattering for a 3″×3″ NaI Detector in Five Configurations 31

TABLES

Table 1. Photon Scatter Distance Distribution 13
Table 2. Environment File Definition 22
Table 3. Heights, Distances, and Wall Distances used in Room Scatter Parameterization 24

NOMENCLATURE

GADRAS	Gamma Detector Response and Analysis Software
1D	one dimensional
3D	three dimensional
GF	Green's Function
keV	kilo-electron-volt (unit of energy)
MeV	mega-electron-volt (unit of energy)
NaI	sodium iodide detector
1x1 NaI	sodium iodide detector with crystal 1-inch in diameter and 1-inch in height
3x3 NaI	sodium iodide detector with crystal 3-inches in diameter and 3-inches in height
HPGe	high-purity germanium detector
60% HPGe	high-purity germanium detector with 60% efficiency relative to a 3x3 NaI

1 INTRODUCTION

The one-dimensional (1D) radiation transport models used in the Gamma Detector Response and Analysis Software (GADRAS) [1] facilitate fast (in a few seconds) computation of radiation sources and shielding configurations. Using a combination of 1D deterministic (S_N) transport simulations and ray-tracing, GADRAS estimates the photon and neutron leakage currents from the surfaces of spheres, cylinders, and slabs. Folding the leakage current with semi-empirical detector response functions produces a detector signal that simulates observable experimental data. Fast computation is ideal for inject studies, inverse transport modeling [2], and computer-resource-limited scenarios such as a laptop environment.

Radiation that leaks from the source directly toward the detector usually dominates the detector signal. Indirect contribution from radiation scattered in the surrounding environment (e.g. floors, walls, surrounding air) is a three-dimensional (3D) radiation transport problem. A simple depiction of the direct and indirect components is shown in **Error! Reference source not found.**. Unfortunately, traditional 3D transport methods (3D deterministic or Monte Carlo methods) lengthen computation time and are incompatible with the purpose and ideology of GADRAS. GADRAS addresses the long computation time by using empirical functions for photons and pre-computed scattering response functions for neutrons. This paper formalizes an approach to photon scattering, describes its implementation in GADRAS, and provides benchmark results against experimental data.

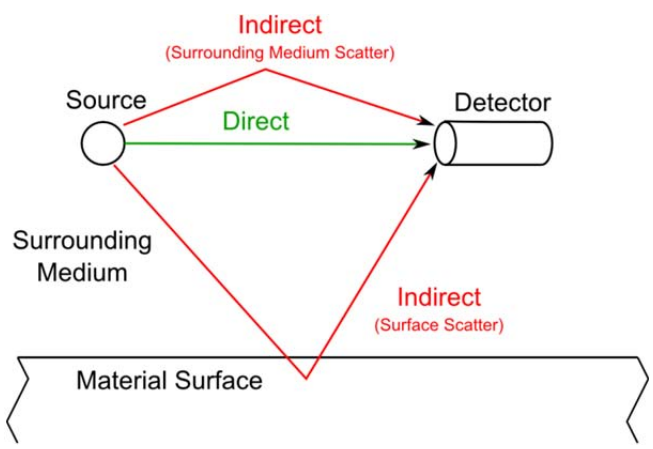

Figure 1. Direct and Indirect Radiation Paths

2 METHODOLOGY

2.1 Green's Functions

Using Green's Functions, also known as response functions or point kernels, GADRAS accounts for the environmental scattering effect. Green's Functions (GFs) describe the response of a system to an excitation. GFs are described mathematically by beginning with the time-dependent Boltzmann transport equation, which dictates the transport of neutral particles in an infinitesimal volume of phase-space,

$\{rate\ of\ change\} = \{production\} - \{attenuation\} - \{leakage\}$,

$$\left\{\frac{1}{v}\frac{\partial \psi}{\partial t}\right\} = \{\boldsymbol{q_{ex}} + \boldsymbol{q_s} + \boldsymbol{q_f}\} - \{\boldsymbol{\sigma_t \psi}\} - \{\boldsymbol{\widehat{\Omega}} \cdot \boldsymbol{\nabla \psi}\}, \tag{1}$$

where $\psi = \psi(\vec{r}, t, E, \widehat{\Omega})$ is the particle flux ($cm^{-2} \cdot s^{-1} \cdot eV^{-1} \cdot str^{-1}$) in the volume d^3r about $\vec{r}$ (cm) traveling in direction $d\widehat{\Omega}$ about $\widehat{\Omega}$ (steradians, str) with energy between E and $E + dE$ (electron-volts, eV) at time t (seconds, s), $v = v(E)$ is the velocity of the particle in ($cm \cdot s^{-1}$), σ_t is the total attenuation cross section in (cm^{-1}), and q_{ex}, q_s, and q_f are source terms from external sources, scattering, and fission, respectively, in ($cm^{-3} \cdot s^{-1} \cdot eV^{-1} \cdot str^{-1}$). Except for very simple problems, there is no analytic solution to this hyperbolic differential equation, hence the need for programs like GADRAS to simulate the physics and transport necessary to approximate its solution.

Let L be the differential operator such that it satisfies the equation

$$\boldsymbol{L\psi} = \boldsymbol{q_{ex}}. \tag{2}$$

Thus, L is the attenuation, streaming, scattering, and production terms from Equation 1. Furthermore, let λ represent the phase-space of the source term such that $d\lambda = d^3\vec{r}\ dt\ dE\ d\widehat{\Omega}$. Generalizing the source term in this equation is accomplished by replacing q_{ex} with the Dirac delta function about phase-space, and replacing the particle flux ψ with the Green's Function G,

$$\boldsymbol{LG}(\boldsymbol{\lambda}; \boldsymbol{\lambda}') = \boldsymbol{\delta}(\boldsymbol{\lambda} - \boldsymbol{\lambda}'). \tag{3}$$

Therefore, the source is now a general point function about phase-space λ'. If the solution to G is known, then the particle flux (response of the system), to any source (excitation of the system) is calculated by integrating over all phase-space of the source Λ,

$$\boldsymbol{\psi} = \int_{\boldsymbol{\Lambda}} \boldsymbol{d\lambda' G}(\boldsymbol{\lambda}; \boldsymbol{\lambda}')\boldsymbol{q_{ex}}(\boldsymbol{\lambda}'),\ \boldsymbol{\lambda}' \in \boldsymbol{\Lambda}. \tag{4}$$

The benefit of the GF method is that the computation time is pushed up-front in the calculation of G, and the computational evaluation of the integral in Equation 4 is trivial compared to solving Equation 2. Furthermore, because the GF contains the full phase-space λ, it may be used to encapsulate 3D transport problems. However, this method rests on "knowing" what G is.

As was the case for Equation 2, analytical solutions to Equation 3 are derivable only for very simple problems. In a computational implementation, expressions for G are usually described in a discretized phase-space.

Furthermore, although solving Equation 4 is fast compared to radiation transport, the expanded form contains an integral for each component of phase-space. The dimensionality of the phase-space, and thus the number of integrals, may be reduced by assuming independence between dimensions and pre-integrating over portions of the phase-space which are approximately uniform in distribution. This pre-integration does not change the full phase-space or accuracy of the radiation transport encapsulated within the Green's function; it only reduces the computation time and storage space required by their application. Improper pre-integration or incorrect assumptions regarding the GF distribution in a phase-space dimension may impede accuracy. Discretizing and reducing the dimensionality of phase-space requires forethought and insight into the radiation transport, and is application-dependent. We now focus on how discretization and reduction may be applied to photon environmental scattering.

2.2 Application of Green's Functions to Surface Scattering

Radiation incident on a scattering surface may take many paths. If it is not absorbed it may be re-emitted at a different angle, energy, position, and time. For now, we assume a steady-state scenario with time-independent GF. To further reduce the dimensionality of the scattering surface GF, we attempt to remove spatial-dependence by assuming any re-emitted particles emerge from the same incident position on the surface.

Assume the worst case scenario: the radiation incident on the scatter surface is at a glancing angle, thus providing the maximum probability that it will diffuse away from the initial point of contact and re-emit at a different position. To test this, a simple MCNP [3] calculation is run in which a pencil beam of photons with energy ranging from 1 keV to 11 MeV is incident on an infinite slab of dirt at a 10 degree angle. The surface is segmented into rings to tally the re-emitted particles as a function of distance from the incident position on the surface. The results are shown in Figure 2. The ordinate is the distance from the incident point on the slab of dirt, the abscissa is the incident energy, and the colors correspond to the probability of emission.

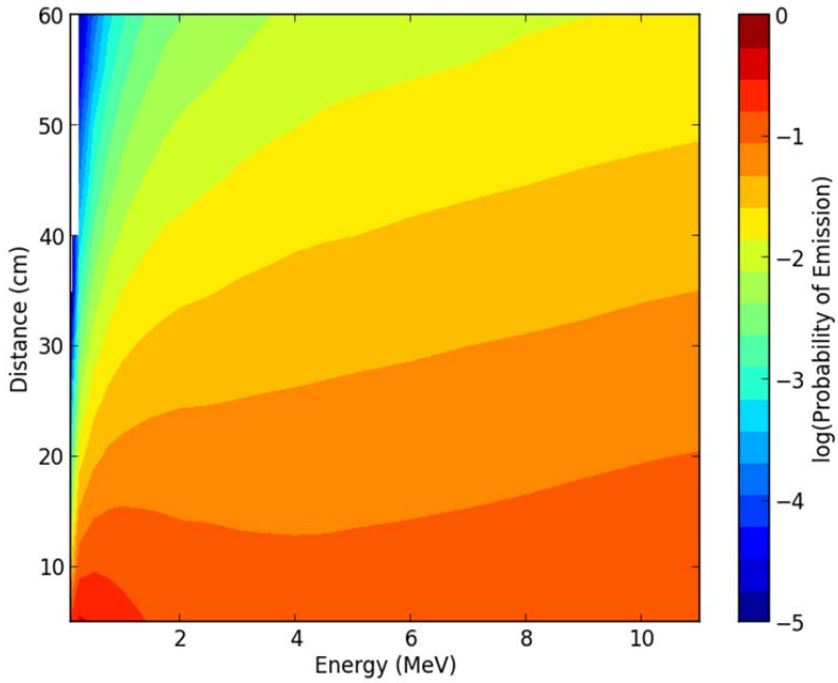

Figure 2. Photon Scattering Distance and Incident Energy

Table 1. Photon Scatter Distance Distribution

	10 Degrees	45 Degrees	90 Degrees
50%	22 cm	15 cm	13 cm
75%	34 cm	23 cm	19 cm
90%	48 cm	34 cm	27 cm

Figure 2 illustrates that the majority of reflected particles occur close to the incident point on the surface. Over 90% of the re-emission occurs within 48 cm. This simple simulation is repeated for a 45 degree incident angle, and a 90 degree incident angle, with emission distribution summarized in Table 1. An upper limit of 50 cm can be established for a dirt slab to capture 90% of all re-emissions. For most grounds, ceilings, walls, and other surfaces of interest, 50 cm is a relatively small area. Therefore, it is a reasonable approximation that any scattered radiation is re-emitted at the same incident point on the surface, thus removing spatial dependence from the reflection GF.

With spatial and time dependence removed, the two remaining densities of the flux are about energy and angle. These two are closely related based on conservation of energy and momentum. Using classical two-body scattering mechanics, the change in energy from a single scatter is only a function of the change in angle between the incident particle and scattered particle, $\Delta\theta$, as shown in Figure 3. In other words, if the polar axis is in the direction of initial flight, then the scattered radiation is uniform in the azimuth, ϕ. In some rare cases, the scattered particle will be dependent on ϕ.

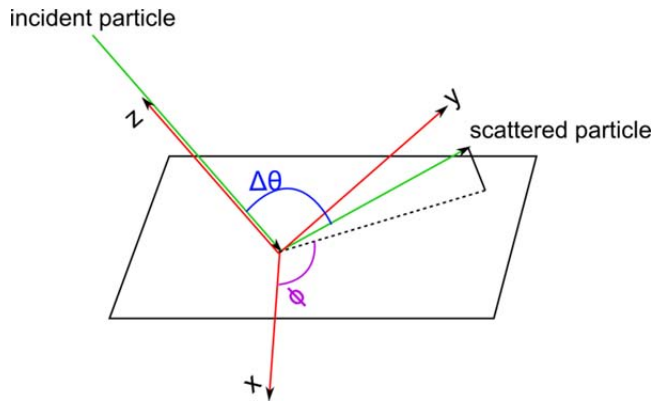

Figure 3. Scatter Angle Dimensions

Surface scattering allows the possibility of multiple scattering events. For multiple scatters, the radiation field cannot be uniform in ϕ unless the incident radiation is perpendicular to the surface. However, discretizing the GF over two angular dimensions is undesirable as it adds another dimension to the integration, increasing computation time. Therefore, it is assumed that the GF is dominated by single-scattering and thus approximately uniform in azimuth.

With these assumptions, the GF may be integrated over space, time, and azimuth, leaving only energy, incident angle, and the change in angle as the remaining dimensions. This is depicted in Figure 4. The functional form to calculate the scattered particle density from the surface is

$$\boldsymbol{N(E,\theta_d) = \int_0^{\pi} d\theta' \int_0^{\infty} dE' G(E' \to E; \theta' \to \theta_d) q(E_s, \theta_s) \delta(E' - E_s) \delta(\theta' - \theta_s),} \tag{7}$$

$$\forall \boldsymbol{E} \in [\boldsymbol{0}, \infty), \qquad \forall \boldsymbol{\theta_d} \in [\boldsymbol{0}, \boldsymbol{\pi}]$$

where $N(E,\theta_d)$ is the particle density in $(s^{-1} \cdot rad^{-1} \cdot eV^{-1})$ toward the detector, $q(E_s,\theta_s)$ is the source at energy E_s and at incident angle θ_s.

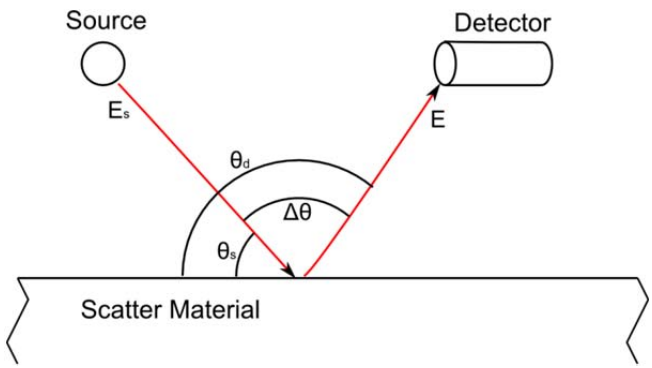

Figure 4. Single Scattering Position on Surface

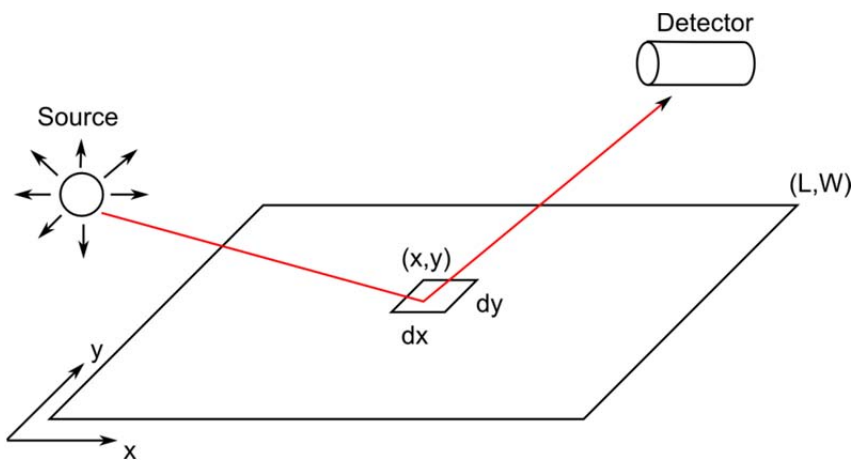

Figure 5. Integration of Scattering Surface

2.2.1 Single Surface Scattering

In reality, pencil beam sources do not exist. Most sources are isotropic, emitting into 4π and striking a scattering surface at multiple positions. Equation 7 is applied to this situation by integrating over the surface as shown in Figure 5. The integration equation is

$$\boldsymbol{C(E) = \int_0^W dy \int_0^L dx \frac{\Omega_s}{4\pi} \int_0^\pi d\theta \frac{\Omega_d}{4\pi} \delta(\theta_d - \theta)} \\ \boldsymbol{\times \int_0^\infty dE' \int_0^\pi d\theta'\, G(E' \to E; \theta' \to \theta) q\,(E') \delta(\theta_s - \theta'),} \tag{8}$$

where $q(E)$ is the source spectrum in $(s^{-1} \cdot eV^{-1})$, $C(E)$ is the detector signal in $(s^{-1} \cdot eV^{-1})$, Ω_s is the solid angle subtended by the surface area $dx \times dy$ about (x, y) on the surface from the source, and Ω_d is the solid angle subtended by the detector from the surface area $dx \times dy$ about (x, y). Although the scattered radiation is not isotropic and the solid angle fraction of $\Omega/4\pi$ does not apply, it is assumed that the radiation field is approximately uniform about θ_d, which should be valid as long as the detector is not too close to the surface. Therefore, taking the contribution

from the scattered source at a single angle θ_d, and applying a correction for the actual solid angle subtended by the detector should yield the approximate probability of striking the detector.

As with volumetric scattering, the energy dimension is cast into N finite groups with $N+1$ group bounds. This allows the source and detector signal to be cast into vectors with length N. The source angle and detector angles are sampled at I and J discrete angles, respectively. This casts the GF into a more abstract 4-dimensional transformation ($G \in R^{N \times N \times I \times J}$) which is not as easily visualized as the energy-only transformation in Equation 6. It serves little purpose then to rewrite Equation 8 in an equally complex form; the continuous energies are collapsed into groups and angles made discrete in Equation 8. The GF at angles between the discrete angles may be estimated by interpolation. The integration over the surface is accomplished by meshing the surface into a grid and using any numerical integration technique. This integration may be repeated as many times as the number of surfaces present in the problem, provided they are treated independently. For dependent surfaces, however, multiple surface scattering must be considered.

2.2.2 Multiple Surface Scattering

A particle which has undergone multiple surface scattering has scattered off two different surfaces before reaching the detector as illustrated in Figure 6. This is a second-order effect and can be ignored in many cases; however, uncommon scattering environments such as small, enclosed spaces have pronounced multiple surface scattering.

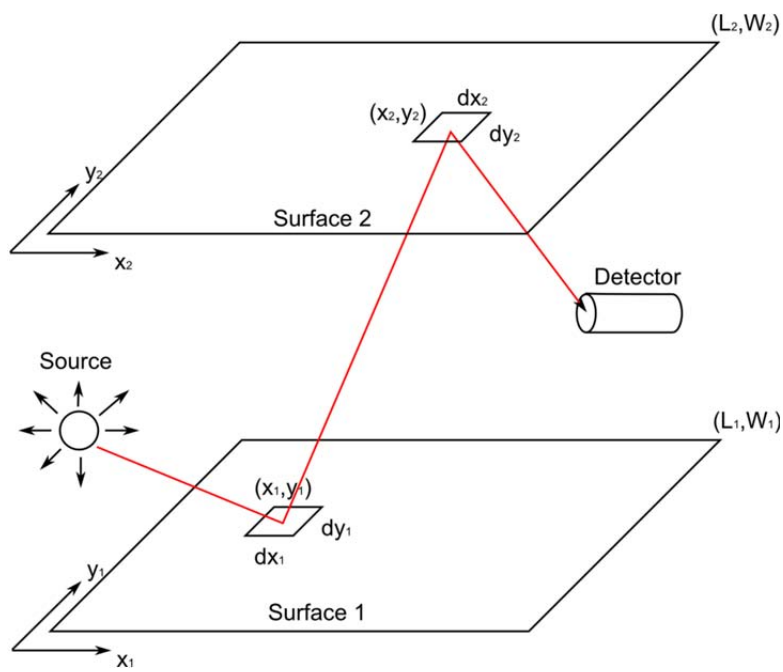

Figure 6. Double Integration of Two Scattering Surfaces

This effect is accounted for by using two GFs for a single scatter on two different surfaces, and calculating a double integration over each surface,

$$
\begin{aligned}
\boldsymbol{C(E)} = \int_0^{W_2} \boldsymbol{dy_2} \int_0^{L_2} \boldsymbol{dx_2} \frac{\boldsymbol{\Omega_{1\to2}}}{\boldsymbol{4\pi}} \int_0^{\pi} \boldsymbol{d\theta_2} \frac{\boldsymbol{\Omega_{2\to d}}}{\boldsymbol{4\pi}} \boldsymbol{\delta(\theta_{2\to d} - \theta_2)} \\
\times \int_0^{\infty} \boldsymbol{dE_1} \int_0^{\pi} \boldsymbol{d\theta_1\, G_2(E_1 \to E; \theta_1 \to \theta_2)\, \delta(\theta_{1\to2} - \theta_1)} \\
\times \int_0^{W_1} \boldsymbol{dy_1} \int_0^{L_1} \boldsymbol{dx_1} \frac{\boldsymbol{\Omega_{s\to1}}}{\boldsymbol{4\pi}} \int_0^{\pi} \boldsymbol{d\theta_1} \frac{\boldsymbol{\Omega_{1\to2}}}{\boldsymbol{4\pi}} \boldsymbol{\delta(\theta_{1\to2} - \theta_1)} \\
\times \int_0^{\infty} \boldsymbol{dE_0} \int_0^{\pi} \boldsymbol{d\theta_0\, G_1(E_0 \to E_1; \theta_0 \to \theta_1) q\,(E_0) \delta(\theta_{s\to1} - \theta_0)},
\end{aligned}
\tag{9}
$$

where $\theta_{s\to1}$ is the angle between surface 1 and the vector from the source and the point (x_1, y_1) in radians, $\theta_{1\to2}$ is the angle between surface 2 and the vector from point (x_1, y_1) to (x_2, y_2) in radians, $\theta_{2\to d}$ is the angle between surface 2 and the vector from point (x_2, y_2) and the detector in radians, $\Omega_{s\to1}$ is the solid angle subtended by the area $dx_1 \times dy_1$from the source in steradians, $\Omega_{1\to2}$ is the solid angle subtended by the area $dx_2 \times dy_2$ from the area $dx_1 \times dy_1$ in steradians, and $\Omega_{2\to d}$ is the solid angle subtended by the detector from the area $dx_2 \times dy_2$ in steradians. The double scatter Equation 9 is essentially an extension of the single scatter Equation 8; and, in principle, the number of scatters that can be computed as an additional layer of integration is unlimited. However, there are computational limitations.

2.2.3 Computational Limitations

Consider a general problem with N surfaces. For simplicity, assume each surface is meshed for numerical integration using the same number M mesh points. The computation time required to compute a single scatter off each surface is proportional to $N \times M$. The time to compute all possible double scatters is proportional to $N(N-1)M^2$. In general, if a photon scatters off K surfaces, the computation time t is

$$
\boldsymbol{t \propto \sum_{k=1}^{K} N(N-1)^{k-1} M^k} \tag{10}
$$

Therefore, of the increased number of mesh points and scatters will result in geometric growth in computation time. To put this into context, for a six surface room (walls, floor, and ceiling) with a modest 100 mesh points on each surface, computing two surface scatters requires a factor of 500 more computation time than a single scatter model, and three scatters requires a factor of 250,000 more computation time than the single scatter. Thus, the three-scatter-surface model is not practical for fast computation. In addition, care should be taken to limit the number of surfaces calculated in the problem to those which are important to the problem.

3 IMPLEMENTATION

Almost any 3D radiation transport software can pre-compute the data necessary to compose the surface and volumetric scattering GFs. For this research, MCNP [3] was chosen for its flexibility and to avoid any ray-effects in the rarified media.

3.1.1 Surface Scattering Simulation Data

The source is modeled as a pencil beam 0.0001 cm above the surface of the scattering material directed into the ground at angles 6, 18, 30, 42, 54, 66, 78, and 90 degrees. The source is sampled over a set of discrete energies ranging from 10 keV to 100 MeV. The energy groups for scattered radiation are source-energy-specific structures ranging from 0 to the source energy over 63 groups. Within each structure, the energy groups near the backscatter peak are finer to capture the peak definition. The detectors are modeled as boxes at angles 6, 18, 30, 42, 54, 66, 78, 90, 102, 114, 126, 138, 150, 162, and 174 degrees at a distance of 100 cm from the point at which the source strikes the surface. This distance was chosen based on the simulations that estimated the re-emission is largely confined to 50 cm from the initial source point. Two sides of the front face of each detector box are coincident with adjacent detector boxes. This creates an arch arrangement as depicted in Figure 7. The energy distribution on each front face is multiplied by 4π and divided by the area of the detector face to remove any dependence on solid angle.

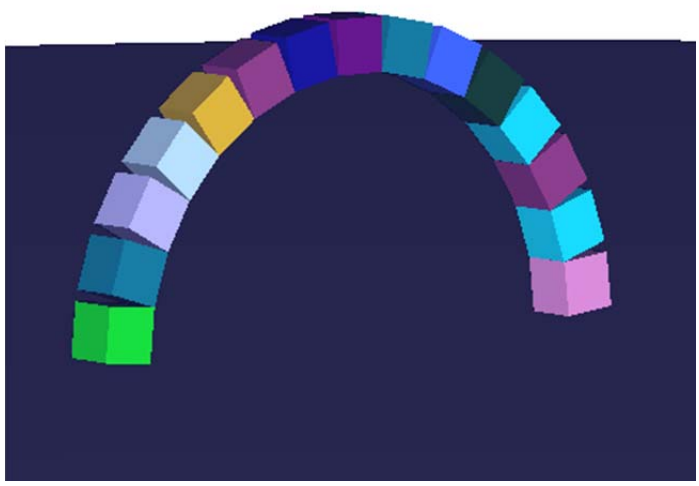

Figure 7. Detector Volume Arch

3.2 Integration into GADRAS

Python scripts were written to parse the MCNP data and produce text files of data. This was converted to a binary format. A module called “Scatter” was written in GADRAS which accepts as input: (1) the source position in three-dimensional space, (2) the detector position, radius, length, and normal vector in three-dimensional space, and (3) any surfaces defined by their

normal, length, width, and material. Surfaces must be rectangular; otherwise, their orientation is not restricted.

To define the limits of integration for Equation 8, the surface is meshed into rectangles based on cast rays, regularly spaced in angle, from the detector face along the length and width of the surface, as illustrated in Figure 8. Along each surface dimension, the angle between adjacent rays is kept constant. The constant angles places smaller mesh rectangles closer to the detector where the solid angle changes more rapidly, and larger meshes farther away where the scatter contribution is less important. In addition, if the surface is small enough or far enough away, this meshing scheme will place a single mesh across the entire surface. This method removes any manual meshing, is flexible to a variety of scatter environments, and reduces computation time caused by an inefficient mesh.

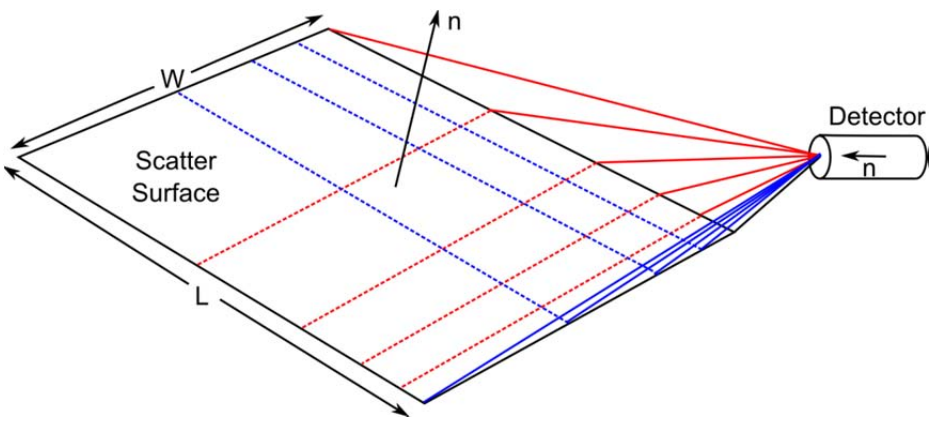

Figure 8. Scatter Surface Mesh

For a double surface integration as shown in Equation 9, the same meshing algorithm is applied, except that the first surface is meshed with respect to the source, while the second surface is meshed with respect to the detector (Figure 9). The automatic meshing attempts to preserve the gradient in the solid angle as a function of position along either surface.

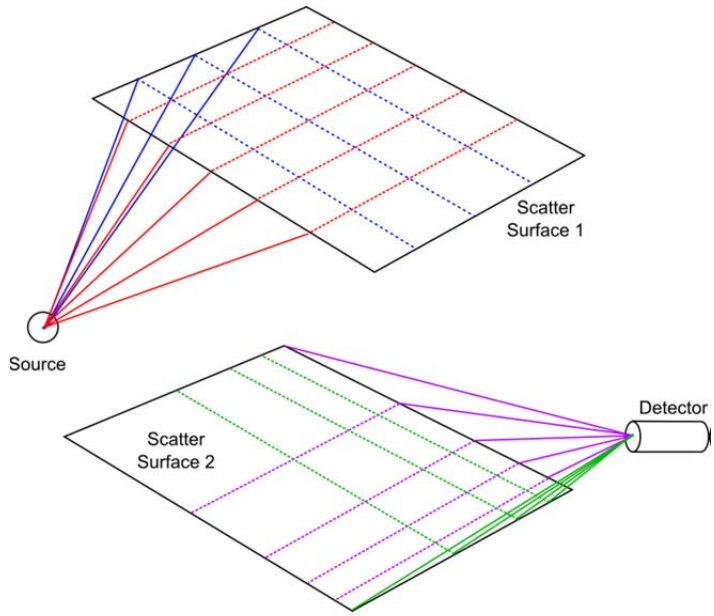

Figure 9. Two Surface Scatter Mesh

The module then parses the necessary binary files for GF data, and integrates by looping over the mesh rectangles, using the center of each as the scatter point. The result of this method is an estimate of the scatter radiation intensity and spectrum on the front, back, and sides of the detector from both the scattering surface and volumetric scattering medium. Aside from the use of interpolation and numerical integration to achieve this result, there are also a few key assumptions and simplifications made.

3.2.1 Solid Angle Computation

To calculate the detector front and back face solid angles from the surface scatter point, it is assumed that the detector faces can be approximated by a square with side length $r\sqrt{\pi}$, where r is the radius of the detector. This approximation preserves the surface area and still allows a solid-angle calculation based on a point to an arbitrarily oriented rectangle.

In calculating the solid angle subtended by the side of the detector, the following equation is used

$$\Omega = \frac{2rL}{4\pi d^2} sin\theta$$

where r is the radius of the detector, L is the length of the detector, d is the distance from the center of the detector to the scatter point, and θ is the angle between the detector normal and the vector from the middle of the detector to the scatter point.

3.2.2 Detector Shielding

As part of the detector response, GADRAS allows users to place attenuators and shielding around the detector. The attenuator and shielding materials are defined by their atomic number

(AN) and the areal density (AD) ($g \cdot cm^{-2}$). There are four main components of the shielding: (1) the inner attenuator which completely surrounds the detection volume, (2) the outer attenuator which completely surrounds the inner attenuator, (3) the side shielding which surrounds the outer attenuator on the sides, and (4) the back shielding which covers the outer attenuator on the back side of the detector. The AN and AD need not be the actual material properties. As many detectors are surrounded by combinations of materials, these need to be only the effective AN and AD.

During the numerical integration of the scattering surface, the radiation intensity on each face of the detector is normalized to the surface area of each respective facet. After the total intensity per unit area on each face is computed, a different GADRAS routine is called to apply any shielding on those faces. This routine assumes that the angular distribution on each surface is uniform. This assumption is valid for typical rooms in which the solid angle subtended by each scattering surface from the detector is large enough to distribute the incoming current in the angular dimension. However, for scattering surfaces that subtend a small solid angle from the detector and create a preferential incident angle of scattered radiation on the detector, this assumption breaks down.

3.2.3 Environment Definition

GADRAS users normally specify distance and height parameters to estimate scattered radiation for a default condition where the source and detector are both located at the same height above the ground plane. A clutter parameter applies an empirical correction to address distances to walls and other objects (see Section 3.2.4). More advanced users can define the scattering environment in detail by writing a file called "Environment.dat" in the detector folder. This is a plain text file which contains keywords followed by numerical data. A description of the file format is summarized in Table 2 which is color-coded to match Figure 10.

Table 2. Environment File Definition

Keyword and Input	Description
SourcePosition s_x s_y s_z	X,Y,Z position of source center
DetectorFace d_x d_y d_z	X,Y,Z position of center of detector face
DetectorNormal n_x n_y n_z	X,Y,Z normal vector describing direction of detector face
Surface	
Type material name	Material the surface is made of (concrete or steel)
Center c_x c_y c_z	Center of the surface
Length l_x l_y l_z	A vector (with magnitude!) of one dimension along the surface plane
Width w_x w_y w_z	A vector (with magnitude!) perpendicular to Length for the other dimension
End Surface	

Most inputs are vectors with three components (x, y, z), which are three numbers separated by a space. The exception is the material name given to the "Type" keyword. The current material options are only "concrete" and "steel." The Surface-End Surface block may be repeated up to ten times to define ten surfaces. Figure 10 illustrates how a single-surface setup may be specified in the file using the keywords. A detector and source are placed on opposite ends of a rectangular

surface, 4 meters apart and 1 meter from the surface. The surface is 2 meters by 4 meters. The detector points directly at the source.

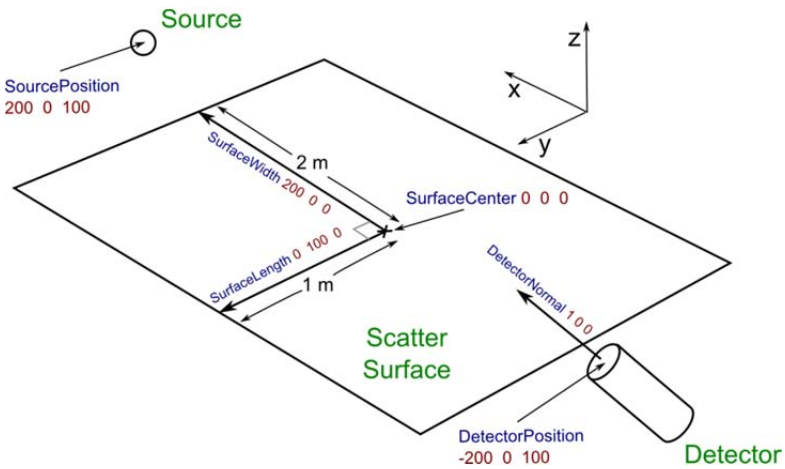

SourcePosition 200 0 100

DetectorFace -200 0 100

DetectorNormal 1 0 0

Surface

Type concrete

Center 0 0 0

Length 0 100 0

Width 200 0 0

End Surface

Figure 10. Environment File and Example Definition

3.2.4 Interpolation Table

Defining surfaces and detector and source positions for each experiment is an onerous task for typical uses, and the efficient computation speed of GADRAS is compromised for multi-surface rooms. Pre-computing typical scenes as a function of distance and height alleviates this issue. Furthermore, distance and height parameters are familiar to GADRAS users. The scene is composed of a room with a concrete floor and ceiling and steel walls. In addition to height and the distance between the source and detector, GADRAS computes scenes with various wall distances. The average wall distance is encapsulated in a single parameter that users can specify whether the source and detector are configured in a large room or a small one. Fully specifying the environment with surfaces and orientations can be done in special cases. If the "Environment.dat" file is present in the detector folder, it will be used for the environment scattering; otherwise, the interpolation method is used.

The appropriate interpolation grid was determined by doing many scatter computations on a large grid to observe trends in the scattered radiation entering the different faces of the detector as a function of the parameterized distances. Figure 11 illustrates the probability per unit area of scattered radiation striking the three detector faces as a function of distance and height for a large room (no walls) and a small room (walls are 50 cm away). When the distance between the source and detector becomes larger than the distance to the walls, the scattering becomes almost independent of source-detector distance. The gradient in the scatter radiation can be quite large for small distances and heights, spanning multiple orders of magnitude between zero and one meter. Based on the exponential gradients observed in Figure 11, linear interpolation is not appropriate for this scheme. Instead, it is better to use a three-dimensional logarithmic interpolation with a finer mesh at small distances and heights to capture the steep gradient.

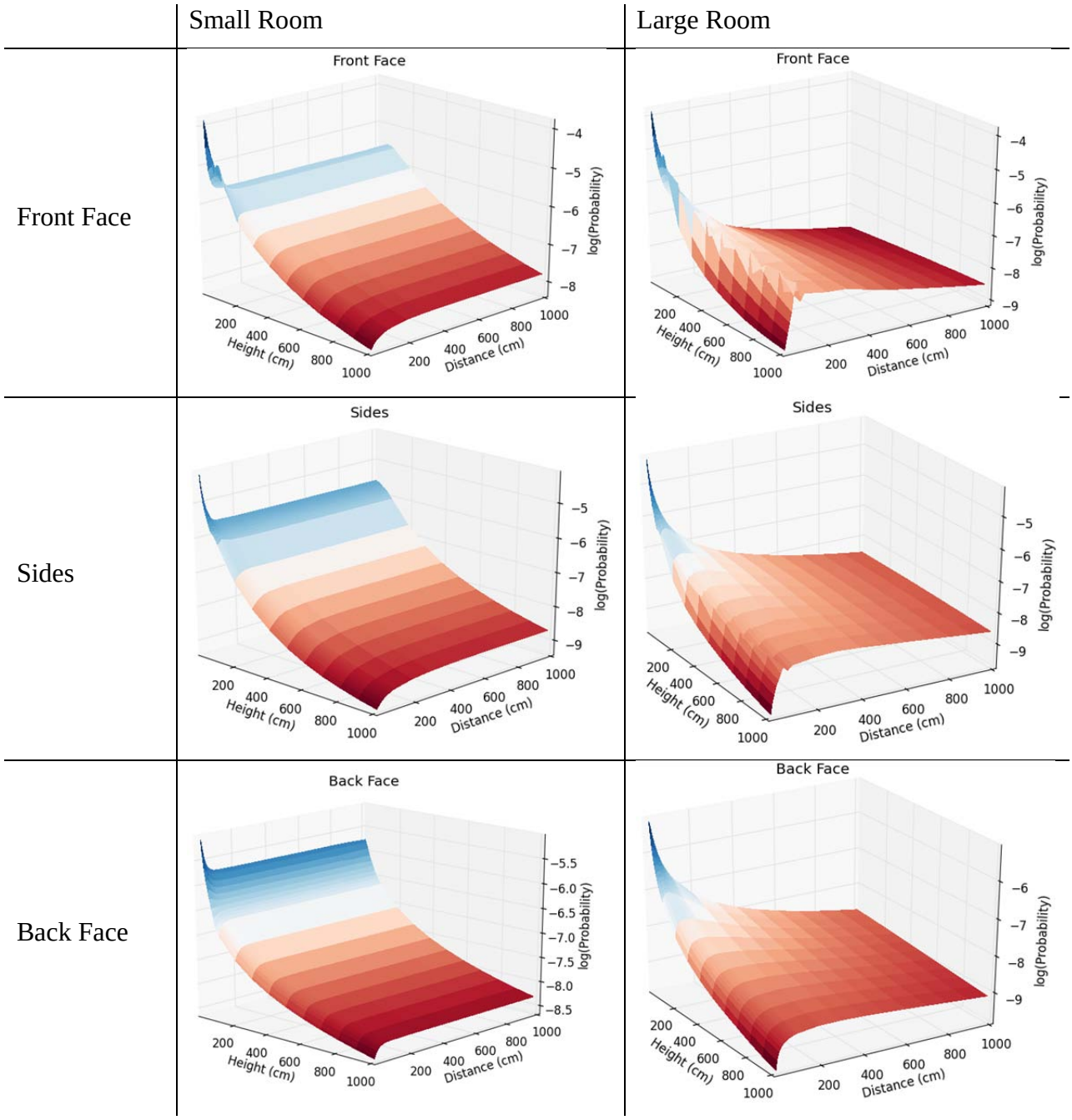

Figure 11. Room Scattering as a Function of Distance and Height

The interpolation points chosen are summarized in Table 3. The scattering function interpolation routine extrapolates for heights and distances specified outside 10 meters. Pre-computed scattering data is written to the "Scatter.gadras" file found in the root structure of the GADRAS folder.

Table 3. Heights, Distances, and Wall Distances used in Room Scatter Parameterization

Heights (cm)	Distances (cm)	Wall Distances (cm)

5	5	10
10	10	50
20	20	100
30	30	200
50	50	500
70	70	No walls
100	100	
140	140	
200	200	
500	500	
1000	1000	

The scatter subroutines use the existing specified distance and height of the source and detector to determine their relative distance and height from the nominal room's floor. To keep the detector characterization parameters consistent with previous versions of GADRAS, the average wall distance is taken from the "clutter" parameter using the formula:

$$\{Wall\ Distance\} = \frac{900\ cm}{\max(\{Clutter\ Term\}, 0.01)}$$

Therefore, when the clutter term is equal to three, the average wall distance is three meters, which is average for a laboratory where detectors are normally characterized. It also limits the clutter term to a minimum of 0.01, equivalent to no walls present. For distances beyond the interpolation table, the energy distribution of the scattered radiation is fixed at the interpolation table's maximum distance, and the intensity is scaled by the squared ratio of the maximum to the actual distance. If the environment file definition is used instead, the clutter parameter is ignored. The remaining scatter parameters are used for both the interpolation table and environment file methods.

3.2.5 User Interface to Scatter Parameters

Aside from clutter, the remaining scatter parameters are:

- 0 Degrees
- 45 Degrees
- 90 Degrees
- 135 Degrees
- 180 Degrees
- Flatten < Edge
- Rate @ E ->0
- Increase with E
- Attenuate

Assigning a nominal value of 3 to all the scatter parameters defines the default scatter environment, which is suitable for bare detectors or detectors that are surrounded by high-atomic-number shields. Although the default settings provide a good starting point when

detectors are characterized, adjustments are generally required to accommodate scattering and variations in shielding within detector housings. The empirical refinement allows flexibility in characterizing a specific detector's configurations and environmental conditions.

The 0-, 45-, 90-, 135-, and 180-degree terms augment or decrease portions of the spectrum corresponding to energy loss from a single scatter at those respective angles. They are incident-energy-dependent, and thus affect different portions of the spectrum depending on the source energy. For example, the 180-degree term changes the magnitude of the backscatter peak at 184 keV from a 661.7-keV source, and the peak at 214 keV from a 1332-keV source. Of course, most sources emit gamma rays at several energies, and these terms account for contributions to the spectrum from all incident photon energies.

Using the scattered radiation model that is described in this paper, the new version of GADRAS has characterized over 100 detectors. The empirical parameters described below provide sufficient flexibility to reproduce observed effects. Due to similarities in the effects on the computed continua, the characterization process can yield non-unique solutions. The best approach for parameter estimation is to first vary the clutter term and the 0-, 45-, 90-, 135-, and 180-degree terms. After these six terms have been fit to the data, the remaining scattered parameters can be allowed to vary to refine the detector response. Described below are the four empirical parameters used to adjust the shapes and energy dependence of radiation continua:

- "Flatten < Edge" affects the low-energy portion of the spectrum. Electronic noise and other phenomena can alter the continuum rate at low energy. Although these effects may not be caused by scattered radiation, distinguish these effects can be difficult, thus they are characterized as if the continuum results from scattered radiation. The energy dependence of the continuum in the low-energy region decreases relative to the default conditions when the value of the "Flatten < Edge" parameter is greater than 3.
- "Rate @ E->0" modifies the slope of the low-energy continuum so that the count rate tends toward zero at the zero-energy limit when the value of the parameter is set at zero. The count rate at low energy increases relative to the default rate when this parameter is greater than 3.
- "Increase with E" determines the degree to which scattering magnitude varies with incident photon energy. Setting the parameter to a value greater than 3 increases the continuum rate derived from high-energy gamma rays.
- "Attenuate" imposes attenuation on the intensity of scattered radiation. This attenuation is based on the energy of the scattered photon, whereas "Increase with E" is based on the energy of the incident photon.

4 TESTING AND BENCHMARKING

In a series of scattering experiments, spectra were recorded with a 3″×3″ sodium-iodide (NaI), a 1″×1″ NaI, and a 60% high-purity germanium (HPGe) detector for several calibration sources. The 3″×3″ NaI detector was used with and without 1.25″ of lead shielding around the sides. The heights ranged from 30 cm to 150 cm, and distances ranged from 50 cm to 200 cm, but the source and detector were always positioned at the same height for most measurements.

Figure 12 compares computed spectra with measurements recorded by the bare 3″×3″ NaI detector at a distance of 100 cm and height of 100 cm. The energy calibration and resolution parameters were adjusted so that computed spectra matched this set of measurements, but the default scatter parameters were applied without adjustment. Good agreement was obtained for all of the detectors over the range of distances and heights explored in this series of measurements. In addition to adjusting energy calibration and resolution parameters, the dimensions of the HPGe detector were also adjusted to match to the measured spectra. The dimensions of the scintillators were asserted without empirical adjustment.

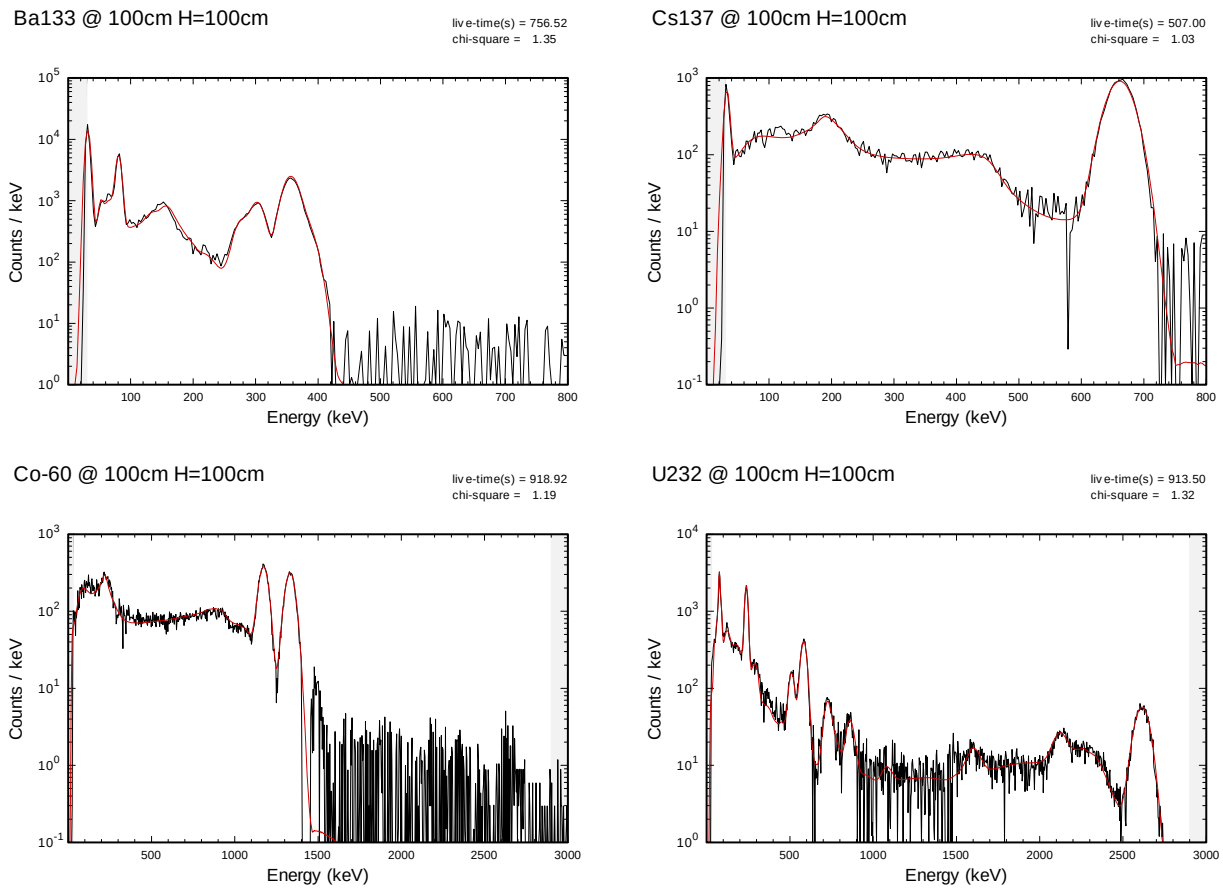

Figure 12. Computed spectra (*red*) for the 3″×3″ NaI detector are compared with measurements (*black*) at a distance of 100 cm and height of 100 cm.

Prior to development of the new scatter model described in this report, the methodology used was to determine a set of empirical scatter parameters that produce a good match between computed spectra and measurements at a specific distance and height. Although this approach enabled calculations with accuracies similar to comparisons shown in Figure 12, the accuracy degraded at conditions different from the calibration configuration. Another limitation with the previous approach is that scatter parameters determined for one detector provided only a rough estimate for the response of another detector under the same conditions. These limitations have been addressed by the new scatter model.

The new model's performance can be evaluated by computing measured spectra with computed spectra for different detectors based on the same set of default scatter parameters (i.e., all of the scatter parameters are set to 3 as discussed in Section 3). Ideally, spectra should be computed accurately for all of the detectors at any distance and height relative to the radiation sources. The degree to which measured spectra can be replicated is illustrated by comparing ^{137}Cs measurements with computed spectra under different sets of controlled conditions. Figure 13 compares spectra for the HPGe detector at three distances and a height of 100 cm. The computed spectra yield good representations of shape and magnitude changes of the spectrum's scattered radiation component. Figure 14 compares spectra where the height changes but the distance is maintained at 100 cm. The final comparison, shown in Figure 15, compares the measured and computed spectra for three of the detectors at the same distance and height. All of the computed spectra agree well with measurements under these detectors, which are effectively bare, but similar agreement cannot be expected for commercial units without characterization of scatter parameters associated with the detector assembly.

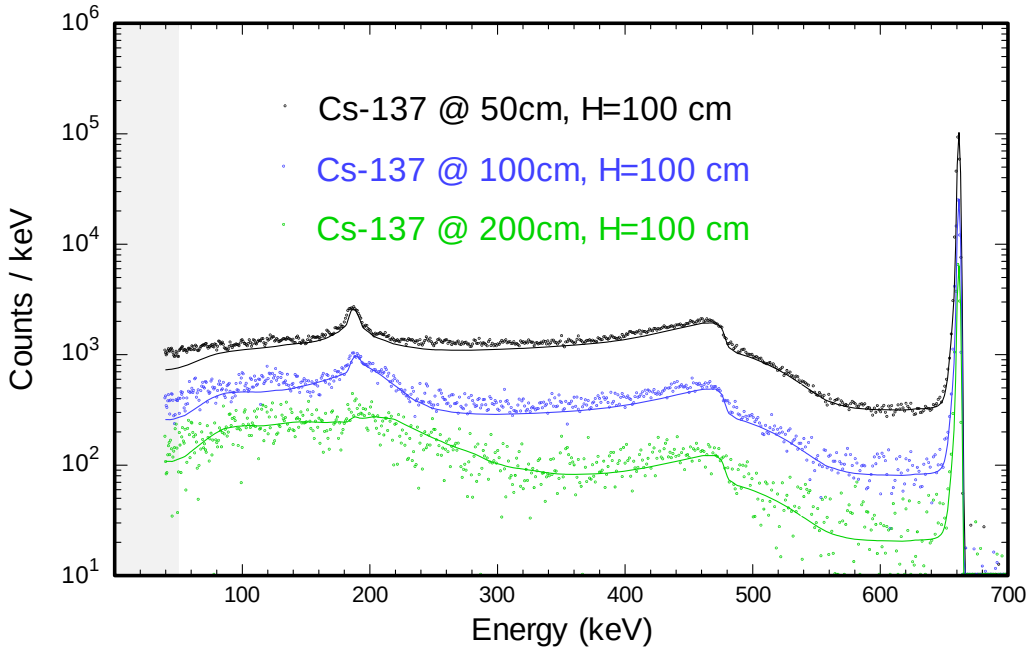

Figure 13. Computed spectra (*lines*) compared with measurements recorded by the HPGe detector at three distances (*dots*) at a height of 100 cm.

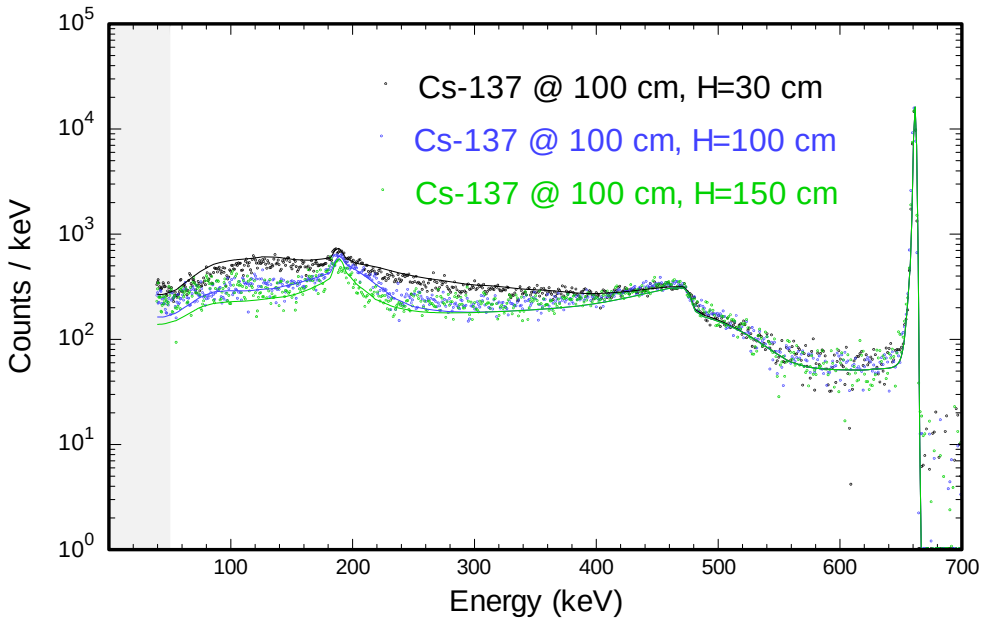

Figure 14. Computed spectra (*lines*) compared with measurements recorded by the HPGe detector at three heights (*dots*) at a distance of 100 cm.

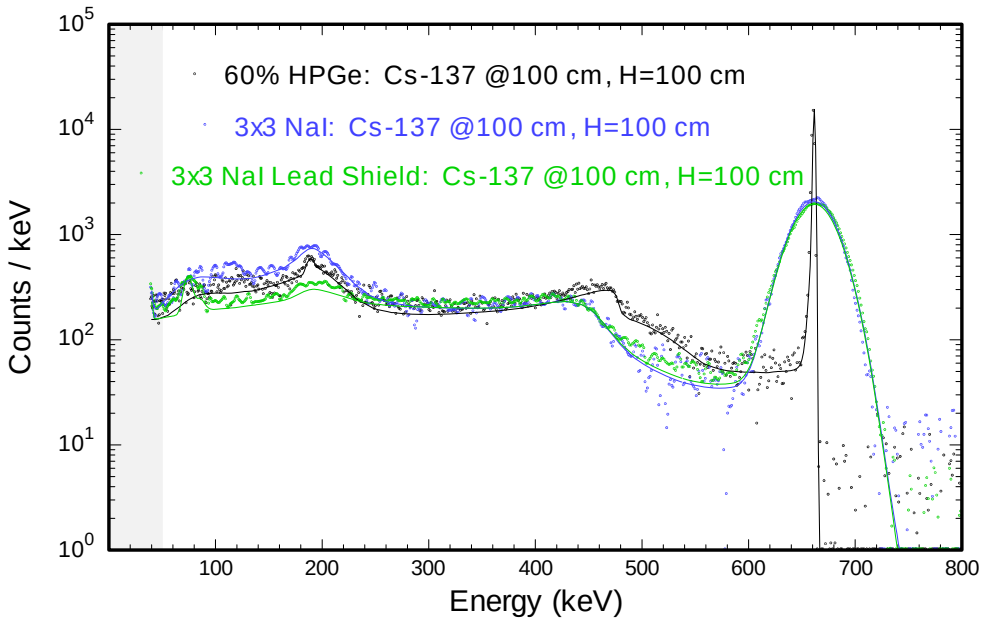

Figure 15. Spectra recorded by the three detectors at the same distance (100 cm) and height (100 cm).

In addition to measurements described above, computed spectra were also compared with measurements collected by a 3″×3″ NaI detector in five additional configurations that test the limits of the new scattering function. The detector response parameters, including those related to scattering, were adjusted to produce the best fit to measurements of all the calibration sources. Figure 16 compares measured and computed spectra for these configurations. Some of these configurations, as noted below, required "Environment.dat" files to characterize the challenging scatter environments.

AboveSource: The source was placed on the ground and the detector, facing downward, was elevated directly above the source. This configuration accentuates the high-angle scattering which is reasonably captured using an "Environment.dat" file.

InCorner: The source was placed in a corner with the detector elevated and looking down into the corner at the source. One wall was brick, the other wall was cinderblock, and the ground was covered with asphalt. This configuration creates a large amount of scatter radiation and multiple-surface scatters. An "Environment.dat" file was created for this scenario as it is not adequately described by the interpolation tables. The shape of the scattering continuum is in error; however, the magnitude is generally correct.

LowScat: Represents a minimal scattering configuration with the source and detector elevated off the ground almost two meters outdoors ("NaI LowScat"). The fit is good especially considering the interpolation tables were used.

MidScat: The result of elevating the source and detector half a meter from the ground indoors ("NaI MidScat"). This is an average configuration one might encounter in an experiment.

OnGround: Figure 16(*e*) corresponds to placing both the detector and the source on the ground one meter apart ("NaI OnGround"). This configuration produces a large degree of low-angle scattering which is accurately modeled by the interpolation table.

AboveSource

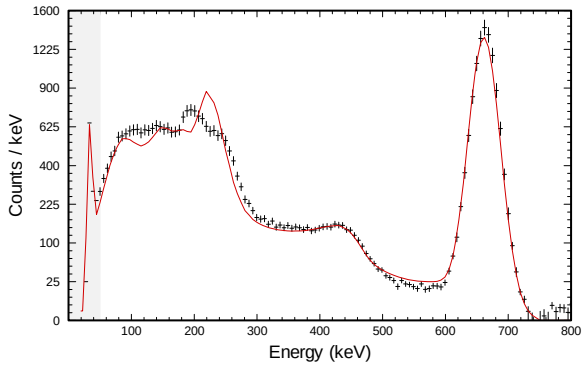

InCorner

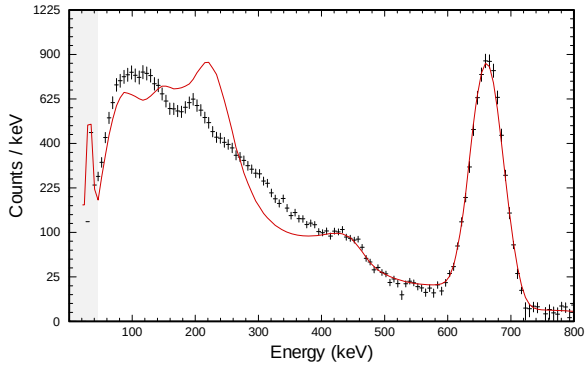

LowScat

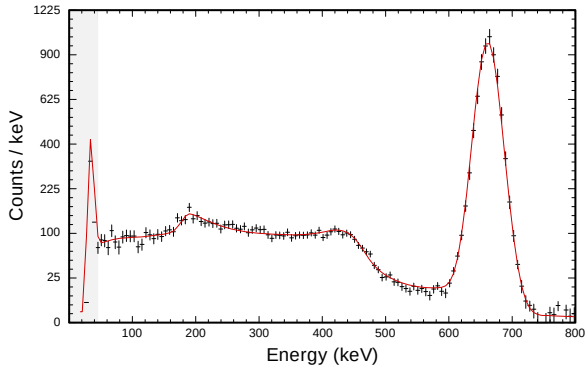

MidScat

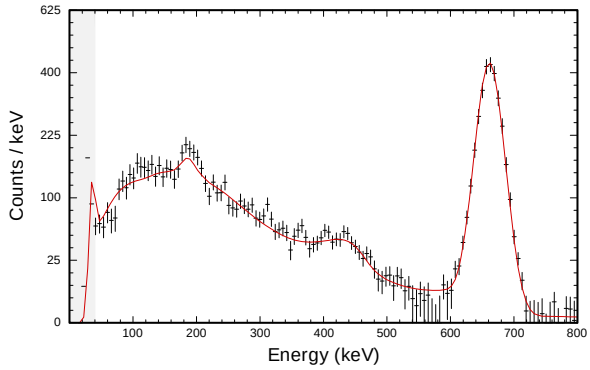

OnGround

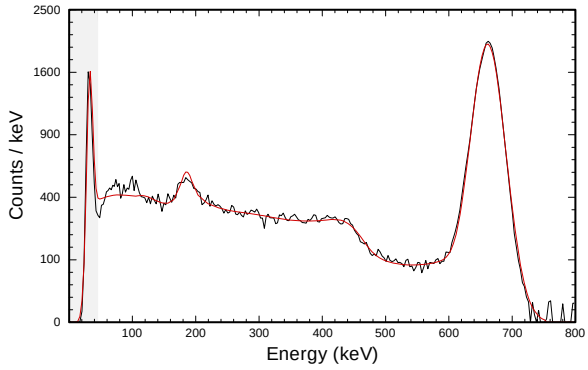

Figure 16. Comparison of Computed versus Measured Scattering for a 3″×3″ NaI Detector in Five Configurations

5 CONCLUSIONS

The Green's Function method was successfully applied to compute the energy distribution of photons from surface scattering. The method was tested against a large set of experimental data with good agreement for most cases. The difference between the simulation and experimental data still grows as the environment is changed from the characterized one; however, it does so more slowly. This allows detectors to be used in a larger variety of environments without re-characterizing them. Furthermore, the predictive modeling capability of GADRAS has been improved by isolating the scattering effects of the environment from scattering within the detector hardware. New scattering functions have been integrated into GADRAS and tested against all detectors distributed with the installer.

6 REFERENCES

1. D.J. Mitchell, Gamma Detector Response and Analysis Software (GADRAS), *Sandia National Laboratories*, SAND88-2519, 1988.
2. J.K. Mattingly and D.J. Mitchell, Implementation and testing of a multivariate inverse radiation transport solver, *Applied Radiation and Isotopes*, 70:1136-1140, 2012.
3. D.B. Pelowitz et. al., MCNPX User's Manual Version 2.6.0, *Los Alamos National Laboratory*, LA-CP-07-1473.

DISTRIBUTION

1	MS0782	Gregory G. Thoreson	6633
1	MS0782	Dean J. Mitchell	6633
1	MS0899	Technical Library	9536 (electronic copy)
1	MS0359	D. Chavez, LDRD Office	1911

Sandia National Laboratories